Phys Chem Minerals (2006) 33: 300–313
DOI 10.1007/s00269-006-0076-z

ORIGINAL PAPER

V. P. Solntsev · E. G. Tsvetkov · A. I. Alimpiev
R. I. Mashkovtsev

# Coordination and valent state of nickel ions in beryl and chrysoberyl crystals

Received: 29 March 2005 / Accepted: 9 February 2006 / Published online: 20 July 2006


**Abstract** We have studied the polarized optical absorption and the EPR spectra of Ni-doped beryls grown by hydrothermal, flux and gas-transport methods, and chrysoberyl grown by the Czochralski and flux methods. In beryls, three groups of bands belonging to three various Ni centres were distinguished by analysis of the absorption band intensities. The first group, bands with maximums at 21740 (**E** ⊥ **c**), 17240 (**E** || **c**) and 9260 (**E** ⊥ + || **c**), 7140 (**E** || + ⊥ **c**) $cm^{-1}$, are due to $Ni^{3+}$ in octahedral $Al^{3+}$ site. The second group is bands at 25640 (**E** ⊥ **c**), 22220 (**E** || **c**) and 13520 (**E** || + ⊥ **c**), 13160 (**E** ⊥ + || **c**) $cm^{-1}$ and 8930 (**E** ⊥ + || **c**), 7460 (**E** || **c**) $cm^{-1}$, which are caused by $Ni^{2+}$ in octahedral $Al^{3+}$ site. Weak wide bands at 17540 (**E** ⊥ **c**), 15500 (**E** || **c**) $cm^{-1}$ and 6580 (**E** || + ⊥ **c**), 5950 (**E** || **c**) $cm^{-1}$ are related to $Ni^{2+}$ in tetrahedral $Be^{2+}$ site. The occurrence of Ni ions in $Be^{2+}$ site is proved by the EPR spectra of $^{1V}Ni^{+}$ in $\gamma$-irradiated samples. According to the spectra of optical absorption of Ni-doped chrysoberyl, two types of Ni centres have been established: $Ni^{3+}$ and $Ni^{2+}$ ions in octahedral $Al^{3+}$ sites. From the EPR spectra of the X-ray irradiated crystals $BeAl_2O_4$: Ni, it follows that 68% of $Ni^{+}$ ions occupy octahedral $Al^{3+}$ sites with mirror symmetry and 32% are in $Al^{3+}$ sites with inversion symmetry. In the approximation of trigonal field with regard to Trees correction, the energy levels of $Ni^{3+}$ and $Ni^{2+}$ have been calculated in octahedral and tetrahedral coordination. There is good agreement between the obtained experimental and calculated data. The polarization dependence of the optical absorption bands is well explained in terms of the spin–orbit interaction.

**Keywords** Beryl · Chrysoberyl · Optical absorption · EPR · Nickel

V. P. Solntsev (✉) · E. G. Tsvetkov · A. I. Alimpiev
R. I. Mashkovtsev
Institute of Geology and Mineralogy SB RAS,
Russkaya st. 43, Novosibirsk 630058, Russia
E-mail: tsvetkov@uiggm.nsc.ru

## Introduction

It was for the first time demonstrated on alexandrite ($BeAl_2O_4$: $Cr^{3+}$) and emerald ($Be_3Al_2Si_6O_{18}$: $Cr^{3+}$) crystals that low-symmetry beryllium-containing crystalline matrices doped with 3*d*-ions are very promising for production of solid-state tuneable lasers (Walling et al. 1980; Alimpiev et al. 1986; Shand and Chine 1982; Gulev et al. 1987). Of particular interest is studying spectroscopic characteristics of other ions from group of iron, including nickel, in these crystal matrixes.

It is known that Ni and Co ions can occupy both octahedral and tetrahedral sites in the beryl and chrysoberyl structures (Solntsev 1981). In this work the valence and coordination of Ni ions in these structures are studied using the EPR and optical absorption spectroscopy.

Beryl ($Be_3Al_2Si_6O_{18}$) is a ring silicate with a hexagonal structure, space group $P6/mcc \equiv D^2_{6h}$ (Morosin 1972), in which $Al^{3+}$ ions are in octahedral coordination, and $Si^{4+}$ and $Be^{2+}$ ions are in tetrahedral coordination. The point symmetry of Si, Be and Al sites is $C_s$, $D_2$ and $D_3$, respectively. The dominant structural units are rings of $Si_6O_{18}$ composition. The rings, arranged in layers in basal plane, are linked laterally and vertically by $Be^{2+}$ and $Al^{3+}$ ions. This stacking arrangement gives rises to the honeycomb-like structure of beryl in which the ring constituents forming the walls of open channels are aligned along the *c*-axis.

Depending upon the conditions of crystal growth, impurity ions may occupy within beryl structure two different sites: octahedral $Al^{3+}$ and tetrahedral $Be^{2+}$ ones. Large impurities, such as alkali metal ions, $CO_3$, $CH_3$, $NH_3^+$ and $NO_3$ radicals, as well as $NO_2$ and $H_2O$ molecules, can be accommodated in the structural channels of beryl matrix (Wood and Nassau 1968; Ginsburg 1955; Goldman et al. 1978; Edgar and Vance 1977; Solntsev 1981; Aines and Rossman 1984; Mashkovtsev and Solntsev 2002). Moreover, the ions of alkali and transition metals can also be found in the

interstitial sites between two $Be^{2+}$ ions with point symmetry $C_{2h}$ or between two $Al^{3+}$ ions with point symmetry $C_{3h}$ (Feklichev 1963; Bakakin et al. 1967). However, this fact is not supported by crystal-chemical data (Aurisicchio et al. 1988). It will be shown below that minor parts of Ni ions (3–5% of the total nickel content in crystal) are, nevertheless, in interstitial positions.

Chrysoberyl ($BeAl_2O_4$) is a hexagonal analogy to the cubic close-packed spinel structure. The oxygen ions form a distorted hexagonal close-packed array in which one eighth of the tetrahedral interstices are occupied by beryllium, and half of octahedral sites are filled with aluminium. In the chrysoberyl structure there are two types of the oxygen octahedra in which the $Al^{3+}$ ions occupy sites with symmetry $C_i$ and $C_s$, whereas the $Be^{2+}$ ions with point symmetry $C_s$ occupy tetrahedral sites with space group $Pnma = D_{2h}^{16}$ (Farrell et al. 1963).

Optical absorption spectra of hydrothermal beryl and chrysoberyl crystals grown from the melt, both doped with nickel ions, are reported in the works of Solntsev (1981) and Gusev et al. (1988), respectively. Three types of Ni centres were revealed in the hydrothermal beryl structure doped by nickel ions: $^{VI}Ni^{3+}$, $^{VI}Ni^{2+}$ and $^{IV}Ni^{2+}$ (Solntsev 1981). However, the detailed analysis of optical spectra of these ions has not been performed as the absorption bands from various Ni ions in octahedral and tetrahedral sites are localized in the regions 6000–8000 $cm^{-1}$ [$^4T_{2g}(^{VI}Ni^{3+})$, $^3T_{2g}(^{VI}Ni^{2+})$, $^3T_2(^{IV}Ni^{2+})$] and 12000–14000 $cm^{-1}$ [$^3T_{1g}(^{VI}Ni^{2+})$, $^3A_2(^{IV}Ni^{2+})$]. The optical spectra of these ions are complicated by additional absorption bands from uncontrolled impurity ($Cu^{2+}$, $Fe^{2+}$). To distinguish the absorption bands of one or another ion in the present work, we investigated the absorption and EPR spectra of beryl crystals grown by hydrothermal, flux and gas-transport methods in which the ratio between different ions was different.

Similar problems arose when interpreting optical absorption spectra of melt-grown $BeAl_2O_4$: Ni crystals. Difficulties in studying these spectra are also due to the superposition of additional absorption bands from $Cr^{3+}$ ions. Therefore, we also studied flux-grown chrysoberyl crystals with different ratio $Ni^{3+}/Ni^{2+}$. To substantiate the correct assignment of the observed absorption bands and their polarization, we have calculated parameters of crystal field of $Ni^{3+}$ and $Ni^{2+}$ ions in the octahedral sites and $Ni^{2+}$ in the tetrahedral site.

## Experimental

The Ni-doped beryl crystals grown by hydrothermal (Lebedev et al. 1988), gas-transport (Rodionov et al. 1987) and flux (Khranenko and Solntsev 1988) methods, as well as Ni-doped chrysoberyl crystals grown by Czochralski (Tsvetkov 1982; Bukin et al. 1981) and flux (Rodionov and Novgorodtseva 1988) methods have been studied by EPR and optical spectroscopy.

The samples for investigation (Table 1) were prepared as oriented platelets polished on both sides. The initial orientation of samples was performed using well-developed faces ($10\bar{1}0$) for beryl and (010), (001) for chrysoberyl crystals. The absorption spectra of the beryl (~10×10×0.3–0.5 mm) and chrysoberyl (~6×5×4 mm) samples in the range of 30000–4000 $cm^{-1}$ were recorded using "SF-20" (LOMO, Russia) and "Shimadzu 3100" (Japan) spectrophotometers in polarized light at 300 K. The EPR spectra of Ni-doped beryl and chrysoberyl samples were recorded at frequency 9.3 GHz and temperatures 300 and 77 K, using a spectrometer "RE-1306" (Institute of Chemical Kinetics SB RAS, Russia). The grown beryl and chrysoberyl crystals were analysed for the stoichiometry of composition, using spectrophotometry and titration method for $SiO_2$ and $Al_2O_3$, respectively, and atomic absorption method supplied with "Perkin-Elmer 400" technique for BeO and microimpurities. Trace oxide contents in crystals were detected by an X-ray microprobe method with a "MS-46 Cameca" (France), with an accuracy ~0.05 wt. %. Results of analyses are given in Table 1.

## Results

### Electron paramagnetic resonance spectra

#### *$Be_3Al_2Si_6O_{18}$: Ni*

The preliminary analysis of EPR data of natural beryl samples has shown the weak spectra from $Cr^{3+}$ (Geusic et al. 1959) and $Fe^{3+}$ ions in them (Dvir and Low 1960), whereas in hydrothermal beryl samples, in addition to the above ions, $Cu^{2+}$ (Solntsev et al. 1976) was also observed.

The EPR spectra of Ni ions were not seen at frequency 9.3 GHz at 77 and 300 K in hydrothermal, flux and gas-transport beryl crystals. However, after $\gamma$-irradiation ($^{60}Co$, $10^7$ rad, 300 K), three additional lines appeared at **H** || **c** caused by three different EPR centres (Fig. 1a). The EPR spectra of flux and gas-transport beryl samples were similar, whereas in $\gamma$-irradiated hydrothermal beryl, additionally, a spectrum from atomic hydrogen was observed (Mashkovtsev and Solntsev 2002). The optical absorption spectra of these samples prior to irradiation are shown in Fig. 3.

The EPR centre (Fig. 1a) represented by an intense line and four weak satellites had three equivalent complexes ($K_m = 3$) in the unit cell. The $X$ axis of each complex coincided with [0001], $Z_1$ with $[2\bar{1}\bar{1}0]$, and $Y_1$ with $[01\bar{1}0]$. The $Z_2$, $Y_2$ and $Z_3$, $Y_3$ axes are turned to $Z_1$ and $Y_1$ axes in plane (0001) at 120° and 240°, respectively. The intensity ratio between the central line and the satellites is roughly 97:1. This is virtually equal to the ratio of the natural content of Ni isotopes with no nuclear spin and that of $^{61}Ni$. The intensity of the satellites increased with increasing Ni. From these facts we concluded that these signals arise from Ni ions, the satellites

**Table 1** Chemical composition of the crystals studied (wt%)

| Sample | Oxides | | | | | | | | | | | |
|---|---|---|---|---|---|---|---|---|---|---|---|---|
| | $SiO_2$ | $Al_2O_3$ | BeO | NiO | $Cr_2O_3$ | $Fe_2O_3$ | CuO | $Li_2O$ | $Na_2O$ | $K_2O$ | $H_2O$ | $\sum$ |
| Hydrothermal beryl | 65.80 | 18.31 | 14.00 | 0.42 | 0.01 | 0.17 | 0.05 | 0.31 | 0.1 | 0.1 | 1.4 | 100.7 |
| Flux beryl | 66.61 | 18.72 | 13.86 | 0.64 | 0.01 | 0.02 | ND | ND | ND | ND | ND | 99.86 |
| Gas-transport beryl | 66.53 | 19.05 | 13.80 | 0.14 | 0.01 | 0.02 | ND | ND | ND | ND | ND | 99.55 |
| Czochralski chrysoberyl | 0.01 | 79.07 | 20.50 | 0.12 | 0.02 | 0.01 | ND | ND | ND | ND | ND | 99.73 |
| Flux chrysoberyl | 0.01 | 80.21 | 19.40 | 0.20 | 0.01 | 0.01 | ND | ND | ND | ND | ND | 99.84 |

*ND* not detected

being the hyperfine structure (HFS) lines of $^{61}Ni$ ($\boldsymbol{I} = 3/2$, natural abundance ~1.25%). The EPR spectra of this centre are described by spin-Hamiltonian ($H$) with spin $S = 1/2$:

$$H = \beta \cdot \boldsymbol{H} \cdot \boldsymbol{g} \cdot \boldsymbol{S} + \boldsymbol{S} \cdot A \cdot I,$$

were $\beta$ is the Bohr magneton, $\boldsymbol{H}$ is the magnetic field, $\boldsymbol{S}$ and $\boldsymbol{I}$ are the electron and nuclear spin operators, $\boldsymbol{g}$ and $\boldsymbol{A}$ are tensors of spectroscopic splitting and HFS, respectively. The angular dependence of lines of this centre is similar to that for ion $Cu^{2+} \rightarrow Be^{2+}$ in beryl structure (Solntsev et al. 1976; Solntsev 1981). Analysis of the EPR parameters of this centre (Table 2) shows that its spectrum is characteristic of the $3d^9$ ion in tetrahedral coordination and is caused by $Ni^+$ ion in the $Be^{2+}$ site.

In a regular tetrahedron of $T_d$ symmetry the $^2D$ term of the $Ni^+$ ion is split into doublet ($E$) and triplet ($T_2$). In the tetragonally $D_{2d}$ distorted four-coordinated complex, the perturbation parameter is given by the angle $\beta$ between the Z-axis of complex and the Ni-ligand vector. According to the deformation angle, we have a regular

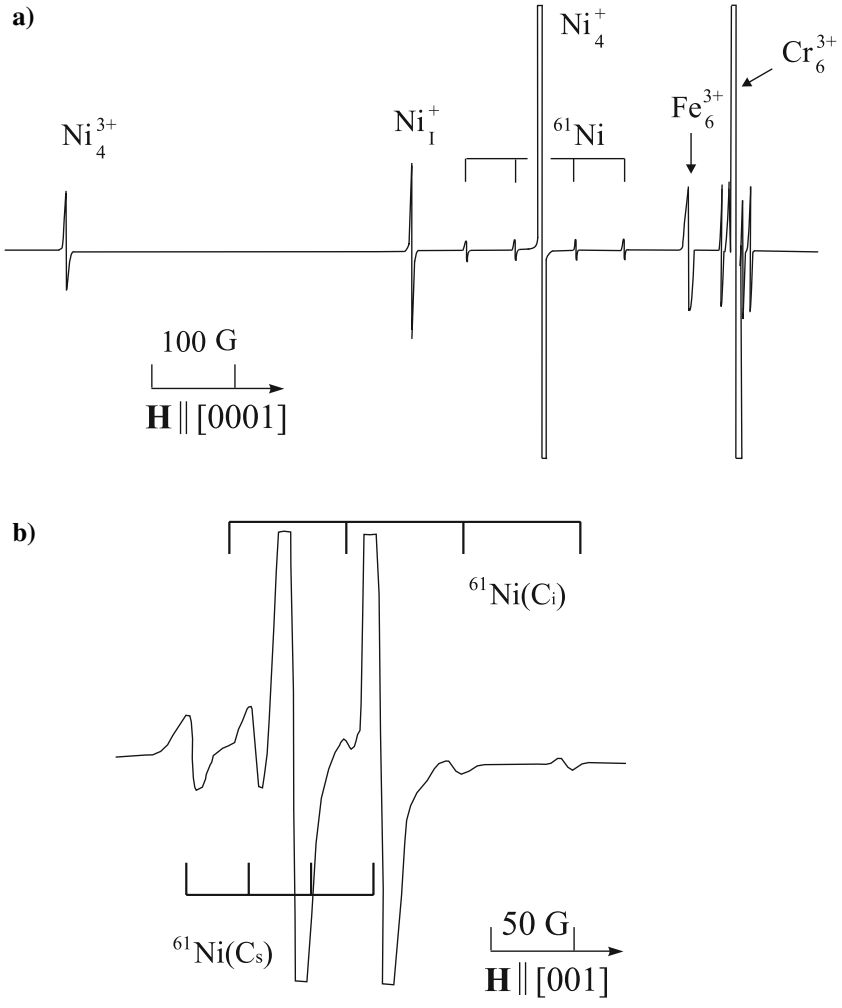


**Fig. 1** EPR spectra of the $Ni^+$ centres in flux beryl (**a**) and chrysoberyl (**b**) crystals formed after an irradiation $\gamma$-ray or X-ray at 300 K (the data were taken at 80 K with the magnetic field parallel to the $c$-axis of the crystals)

**Table 2** Spin-Hamiltonian parameters for the **g** and **A** matrices of the $Ni^{+}$ centres in beryl and chrysoberyl

| Crystal | Ion | $K_m$ | Principal values $g$-tensor ($\pm 0.001$) | Principal-axis directions | | Principal values $A$-tensor ($\pm 0.5\times10^{-4}$ $cm^{-1}$) | Occupied position |
|---|---|---|---|---|---|---|---|
| | | | | $\theta$ | $\varphi$ | | |
| Beryl | $Ni^{+}(4)$ | 3 | $g_z = 2.465$ | 90 | 0 | $^{61}A_c = 62.3$ | $Ni^{+} \rightarrow$ Be |
| | | | $g_y = 2.116$ | 90 | 90 | | |
| | | | $g_x = 2.101$ | 0 | | | |
| Beryl | $Ni^{+}(i)$ | 6 | $g_z = 2.287$ | | | | $Ni^{+} \rightarrow$ I |
| | | | $g_y = 2.140$ | | | | |
| | | | $g_x = 2.124$ | | | | |
| Beryl | $Cu^{2+}$ | 3 | $g_z = 2.359$ | 90 | 0 | $^{63}A_z = 125.6$ | ⑤ |
| | | | $g_y = 2.091$ | 90 | 90 | $^{63}A_y = 15.7$ | $Cu^{2+} \rightarrow$ Be |
| | | | $g_x = 2.071$ | 0 | | $^{63}A_x = 5.0$ | |
| Chrysoberyl | $Ni^{+}(C_s)$ | 2 | $g_z = 2.2520$ | 57 | 0 | $^{61}A_c = 39.6$ | $Ni^{+} \rightarrow Al(C_s)$ |
| | | | $g_y = 2.1184$ | 33 | 180 | $^{61}A_a = 28.9$ | |
| | | | $g_x = 2.1165$ | 90 | 90 | $^{61}A_b = 23.5$ | |
| Chrysoberyl | $Ni^{+}(C_i)$ | 4 | $g_z = 2.0472$ | 58 | 55 | $^{61}A_c = 54.1$ | $Ni^{+} \rightarrow Al(C_i)$ |
| | | | $g_y = 2.1656$ | 72 | 313 | $^{61}A_a = 57.2$ | |
| | | | $g_x = 2.1768$ | 38 | 198 | $^{61}A_b = 14.5$ | |

⑤Solntsev et al. (1976); Solntsev (1981)

tetrahedron ($\beta_T = 54.74°$). When the tetrahedron undergoes elongation ($\beta < \beta_T$), the ground state is $d_z^2$. In the compressed tetrahedron, $d_{xy}$ is the ground state, if $\beta = 54.74$–$90°$ (Hoffmann and Goslar 1982). The $D_2$-rhombic distorted $BeO_4$ complex in beryl ($\beta = 65.7°$) is shown in Fig. 2a. In crystal field of $D_2$ symmetry with the account of spin–orbit coupling, degeneration of levels is completely removed. The ground state of $Ni^{+}(Cu^{2+})$ in compressed tetrahedron will be $d_{xy}$ ($B_1$). Because of the small intensity of EPR lines from $^{61}Ni^{+}$, we could not define principal values of $A$-tensors. Taking into account the similarity of angular dependences of $g$-tensors of $Ni^{+}$ and $Cu^{2+}$, the hyperfine interaction will be analysed on the example of $Cu^{2+}$. Neglecting small anisotropy of

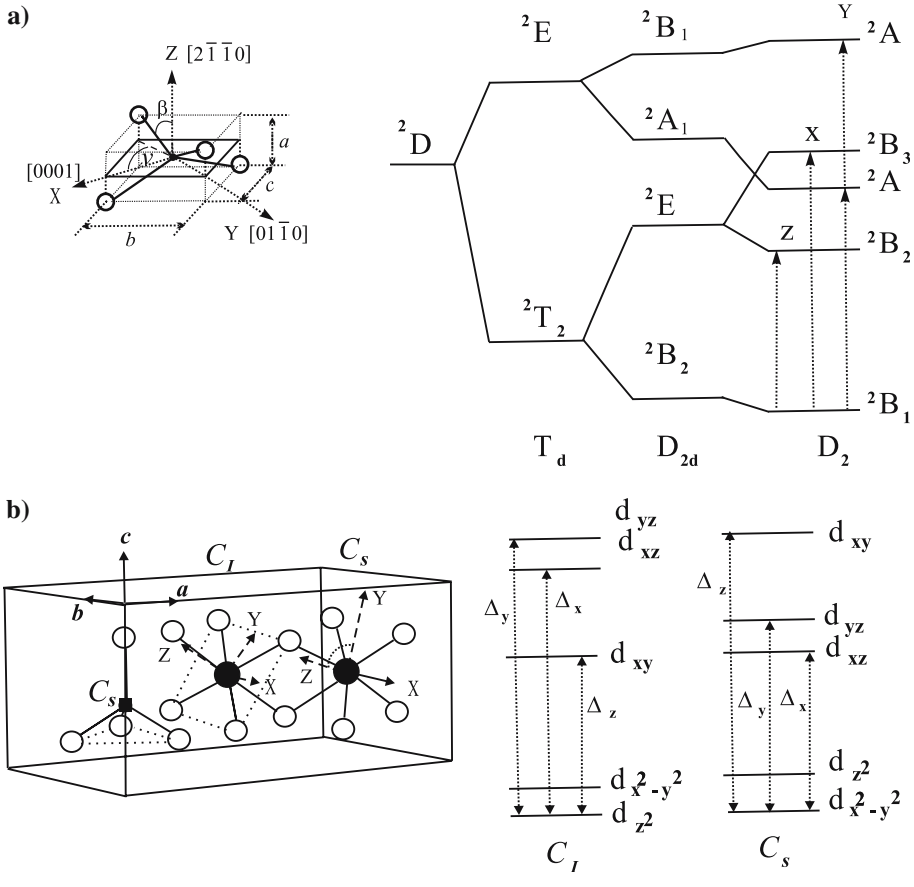


**Fig. 2** Orientation of the axes $g$-tensor $Ni^{+}$ centres relative to the crystallographic axes **a**, **b** and **c** in beryl (**a**) and chrysoberyl (**b**); on the right side of the figure is a scheme of splitting of energy levels of $Ni^{+}$ in tetrahedral (beryl) and octahedral (chrysoberyl) sites at decreasing symmetry of environment

$g$- and $A$-tensors, we shall assume that the EPR spectrum had an axial symmetry.

The ground-state $d_{xy}$ occurs in $D_{2d}$ flattened tetrahedral $Ni^+(Cu^{2+})$ complexes. For this ground state $d_{xy}$ of symmetry $B_2$, the crystal field can admix the state $4p_z$ of the same symmetry. Similar effects of hybridization occur for the states $d_{xz}$, $d_{yz}$ and $4p_x$, $4p_y$. Accordingly, the wave functions now are $\Psi(\boldsymbol{B}_2) = \alpha \boldsymbol{d}_{xy} + \eta P_z$, $\Psi(\boldsymbol{B}_1) = \boldsymbol{d}_{x^2-y^2}$, $\Psi(\boldsymbol{E}) = \gamma \boldsymbol{d}_{xz,yz} + \zeta P_{x,y}$, $\Psi(A_1) = \delta \boldsymbol{d}_{z^2} + \delta_1 \boldsymbol{s}$. Using the theory perturbation in the first and second order Hoffmann and Goslar (1982) has written the following equations spin-Hamiltonian parameters:

$$
\begin{aligned}
g_{\|} &= 2 - 8\,a^2\lambda_d/E_{x^2-y^2},\\
g_{\perp} &= 2 - 2\left(\alpha^2\gamma^2\lambda_d - \alpha\gamma\zeta^2\lambda_p\right)/E_{xz,yz},\\
\mathbf{A}_{\|} &= \mathbf{P}_d[-k\alpha^2 - 4/7\,\alpha^2 + (g_{\|} - 2) - 3/7\,(g_{\perp} - 2)]\\
&\quad + \mathbf{P}_p\eta^2(-k + 4/5),\\
\mathbf{A}_{\perp} &= \mathbf{P}_d[-k\alpha^2 + 2/7\,\alpha^2 + 11/14\,(g_{\perp} - 2)]\\
&\quad + \mathbf{P}_p\eta^2(-k - 2/5),
\end{aligned}
$$

where $\lambda_d = -605\ \mathrm{cm}^{-1}$, $\lambda_p = -705\ \mathrm{cm}^{-1}$ ($Ni^+$) and $\lambda_d = -829\ \mathrm{cm}^{-1}$, $\lambda_p = -925\ \mathrm{cm}^{-1}$ ($Cu^{2+}$) are free-ion spin–orbit constants for $3d$ and $4p$ orbital, respectively. $E_{ij}$ are the energy separations between the ground state ($\boldsymbol{B}_2$) and $d_{ij}$ orbital. $\mathbf{P}_d = 0.0399\ \mathrm{cm}^{-1}$ ($^{63}Cu^{2+}$) and $\mathbf{P}_p = 0.0446\ \mathrm{cm}^{-1}$ are the copper-ion dipolar HFS parameters for $3d$ and $4p$ orbital, and $k$ is the Fermi contact parameter. For the nickel-ion ($^{61}Ni^+$) $\mathbf{P}_d = 0.0112\ \mathrm{cm}^{-1}$ (Morton and Preston 1978). If the $p$-state admixture is negligible ($\eta = \xi = 0$), i.e. when dealing with a purely $d_{xy}$ ground state, the orbital splitting with respect to the ground state of $Ni^+(Cu^{2+})$ ion in beryl is easy to obtain. The calculated values $\Delta_{x^2-y^2} = 14100$ and $\delta_{xz,yz} = 10100\ \mathrm{cm}^{-1}$ are in good agreement with the data obtained from the absorption spectra: $^2B_1 \rightarrow {}^2B_2 = 13300$, $^2B_1 \rightarrow {}^2B_3 = 8500$ and $^2B_1 \rightarrow {}^2\mathrm{A} = 10900\ \mathrm{cm}^{-1}$ (Solntsev et al. 2004).

Evaluation of $\Delta_{x^2-y^2}$ and $\delta_{xz,yz}$ for $Ni^+ \rightarrow Be^{2+}$ from $\Delta g_{\|} = 8\lambda_d/\Delta_{x^2-y^2}$ and $\Delta g_{\perp} = 2\lambda_d/\delta_{xz,yz}$ gives $\Delta_{x^2-y^2} = 10800$ and $\delta_{xz,yz} = 11500\ \mathrm{cm}^{-1}$. As this absorption of $Ni^+$ falls in the area of more intense absorption from the $Ni^{2+}$ and $Ni^{3+}$ ions, it was not possible to distinguish the above bands in optical spectra. Hoffmann and Goslar (1982) have shown that when tetrahedron is compressed (involving an increase in $\beta$ from 54.74 to 90°)—$g_{\|}$, $g_{\perp}$ and $A_{\perp}$ decrease, whereas $|A_{\|}|$ strongly increases. This correlates well with the $g$- and $A$-factors of $Ni^+$ and $Cu^{2+}$ ions (Table 2) in the distorted $BeO_4$ tetrahedron of ($\beta > 66°$) beryl structure. In the square-planar limit ($\beta = 90°$) the changes in $g_{\|}$, $g_{\perp}$ and $A_{\perp}$ are negligible. From comparison $g_{\|}$ and $g_{\perp}$ of $Cu^{2+}$ and $Ni^+$ ions one can see that the deformation angle for $CuO_4$ tetrahedron is bigger than for $NiO_4$ ones.

The centre with $g_c = 2.198$ has six equivalent complexes in an elementary cell and is described by spin-Hamiltonian rhombic symmetry with $S = 1/2$. One of three axes of the centre ($Y$) coincided with $[01\bar{1}0]$, and the others fall in plane $(01\bar{1}0)$. The angular dependence of the centre correlates with the expected angular dependence of $Ni^+$ in position $k$ in beryl structure ($Ni^+(i)$, Table 2). HFS from $^{61}Ni$ ($\boldsymbol{I} = 3/2$, natural prevalence of 1.25%) was not observed owing to the small intensity of the centre.

The centre with $g_c = 2.542$ has three equivalent complexes ($K_m = 3$). Because of the big width of lines and small intensity of the centre, it was not possible to determine its true spin. However, taking into account the amount of complexes, it is possible to assume that the spectrum of the centre is caused by $Ni^{3+}$ ion in the $Be^{2+}$ site. The obtained data are insufficient for unambiguous identification of the centre.

It is worth noting that after a $\gamma$-irradiation ($Co^{60}$, 5–100 Mrad, 77 K) in flux and gas-transport beryl crystals at 80 K we observed two additional EPR centres: $O^-$ that is a "hole" on oxygen of $SiO_4$ tetrahedron in which $Si^{4+}$ is substituted by $Al^{3+}$[$g_c = 2.014$, $^{27}A_c$ (Al) = 7.0, $^9A_c$(Be) = 2.0 G], and the centre $Al^{2+}$ in $Be^{2+}$ site [$g_c = 1.9962$, $^{27}A_c = 391$ G], which were described earlier (Solntsev and Khranenko 1989). The data obtained suggest that the charge of $Ni^{2+}$ lacking in octahedral sites in flux and gas-transport beryl crystals may be compensated by the occurrence of $Al^{3+}$ in the $Be^{2+}$ site.

### *$BeAl_2O_4$: Ni*

Before irradiation, only weak EPR spectra from $Cr^{3+}$ (Forbes 1983; Solntsev 1981) and $Fe^{3+}$ (Barry and Troup 1970) ions were seen in Ni-doped chrysoberyl crystals. The absorption spectra of flux (Fig. 4) and melt (Gusev et al. 1988) Ni-doped chrysoberyl crystals were represented by three groups of bands typical of $Ni^{2+}$ and $Ni^{3+}$ ions in octahedral sites. The spectra differed in that the $Ni^{3+}$ bands in flux samples were more distinct than in melt samples and they lacked additional absorption bands from $Cr^{3+}$ ions. No EPR spectra from Ni ions were observed at frequency 9.3 GHz and at both 77 and 300 K. After an X-ray irradiation (40 kV, 3–10 Mrad, 300 K) of $BeAl_2O_4$: Ni crystals, bands typical of $Ni^{2+}$ slightly decrease in intensity, absorption increases with a maximum $19000\ \mathrm{cm}^{-1}$ and there appears additional intense absorption at $\lambda_{\max} < 25000\ \mathrm{cm}^{-1}$. This suggests that only minor part of $Ni^{2+}$ ions changed valence.

In the EPR spectra of these crystals we observed two additional ($\mathbf{H} \parallel \mathbf{c}$) intense lines with $g_c = 2.1598$ and $g_c = 2.1256$ as well as weak quartet lines located symmetrically against the basic lines (Fig. 1b). The first centre ($g_c = 2.1598$) has two nonequivalent magnetic complexes in a unit cell ($K_m = 2$), whereas the second centre ($g_c = 2.1256$) has four of these. Analysis of the angular dependence of the lines showed that they are due to $Ni^+$ in two different octahedral positions: $68 \pm 2\%$ of $Ni^+$ occupy positions with $C_s$ symmetry and $32 \pm 2\%$ with $C_i$ symmetry

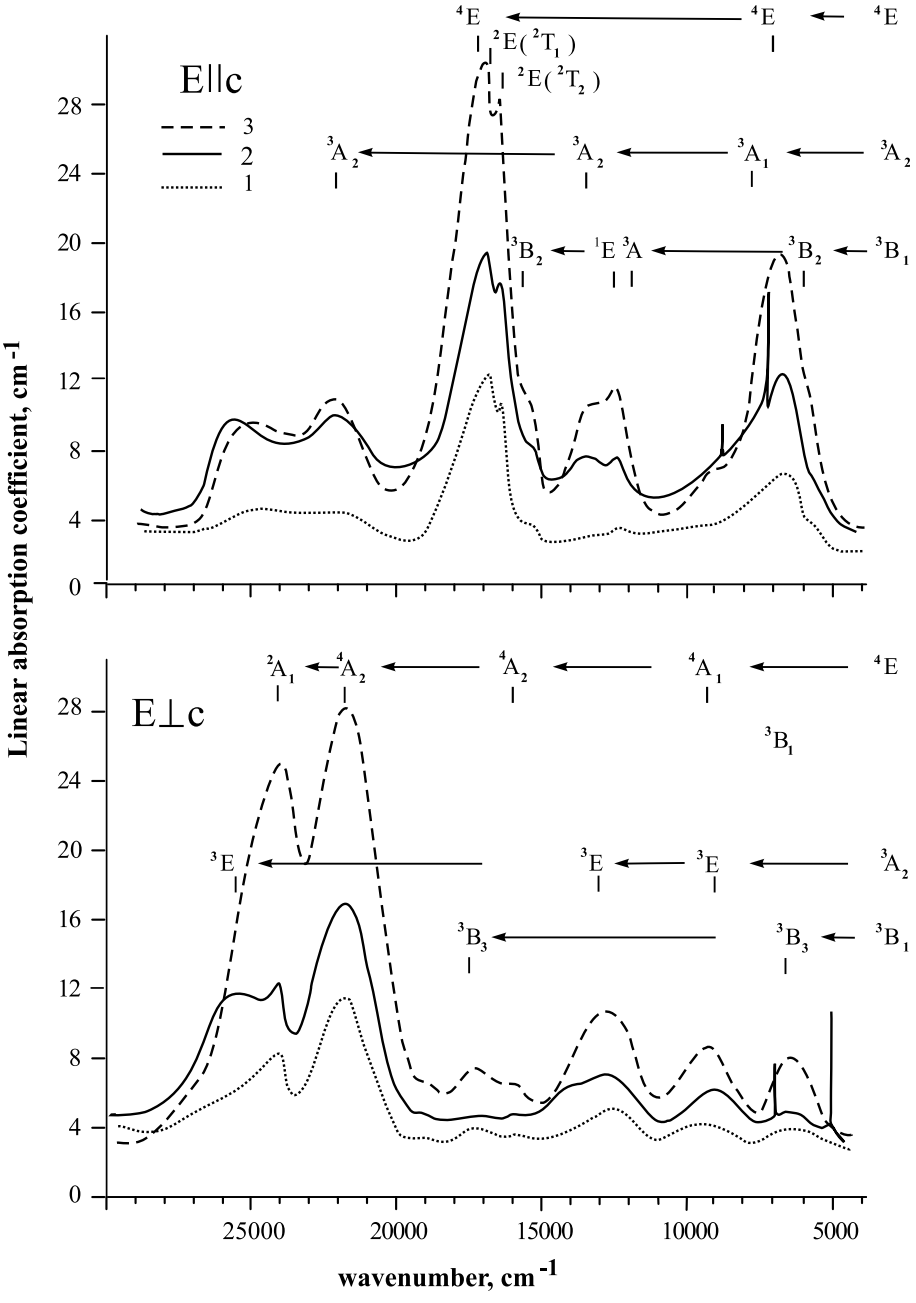


**Fig. 3** Polarized electronic absorption spectra of Ni-doped beryl at 300 K; *1* gas-transport grown beryl, *2* hydrothermal beryl, *3* flux beryl

(Fig. 2b). The weak quartet lines result from the interaction of unpaired $Ni^+$ electron with the nuclear moment of $^{61}Ni$ ($\boldsymbol{I} = 3/2$, natural prevalence of 1.25%). In accordance with $Ni^+$ ($S = 1/2$) occupying the sites of symmetries $C_i$ and $C_s$, two orthorhombic spin-Hamiltonians were used to interpret the EPR spectra. Unfortunately, it was not possible to study the angular dependence of lines HFS in details because of the presence of lines from the $Cr^{3+}$, $Fe^{3+}$ ions and the big number of $Ni^+$ in this site. Therefore, Table 2 shows HFS only along directions [001], [010] and [100].

In chrysoberyl structure $AlO_6$ ($C_s$) octahedron has a tetragonal distortion corresponding to the expansion along the fourth-order $z$-axis (Fig. 2b). As a result of this distortion, the ground state of the ion with the $d^9$ electron configuration is $d_{x^2-y^2}$

(Carrington and McLachlan 1970). A decrease in the symmetry of octahedral complex to $C_i$ leads to the $d_{z^2}$ ground state. Thus, it is apparent that in distorted octahedral nickel complexes an unpaired electron resides in $d_{x^2-y^2}$ or $d_{z^2}$ orbital. The deviations of the $g$ values from the free-electron one are due to the mixing of the ground state with higher excited states. Thus, wave functions are mixed in the ground state and in other states, i.e. for ground state $\boldsymbol{d}_{X^2-y^2}$ ($A_1$): $\Psi(A_1) \alpha \boldsymbol{d}_{X^2-y^2} + \delta \boldsymbol{d}_{z^2} + \eta P_z + \delta_1 \boldsymbol{s}$. Omitting admixtures from $\boldsymbol{p}$ and $\boldsymbol{s}$ orbital and neglecting the $d_{z^2}(d_{x^2-y^2})$ admixtures to the

ground state, Hayes and Wilkens (1964) gave the following expressions for $g$ values. For the ground state $d_{x^2-y^2}$ :

$$g_{||} = 2 - 8\lambda/\Delta_{||} - 3[\lambda/\Delta_{\perp}]^2 - 4\lambda^2/\Delta_{||}\Delta_{\perp} \quad \text{and}$$
$$g_{\perp} = 2.0023 - 2\lambda/\Delta_{\perp} - 4[\lambda/\Delta_{||}]^2;$$

for the ground state $d_{z^2}$ :

$$g_{||} = 2 - 3\,[\lambda/\Delta_{\perp}]^2 \quad \text{and}$$
$$g_{\perp} = 2 - 6\lambda/\Delta_{\perp} - 6\,[\lambda/\Delta_{\perp}]^2,$$

where $\lambda$ is the spin–orbit coupling parameter, the values of the energy distances $\Delta_{||} = \Delta_z$ and $\Delta_{\perp} = \Delta_x + \Delta_y/2$ can be understood from Fig. 2b. These equations allow only a qualitative explanation of the experimental data. For a precise quantitative calculation of the EPR parameters it is necessary to take into account mixing of $d_{z^2}$ and $d_{x^2-y^2}$ and other excited configurations, as well as covalence. Using the above-mentioned expressions for $g$-factors, we can obtain information about the relative positions of energy levels. From the quantities given in Table 2 and taking $\lambda = -450$ cm$^{-1}$ we obtained the values $\Delta_{||} = 13280$ cm$^{-1}$ and $\Delta_{\perp} = 7360$ cm$^{-1}$ for $Ni^{+}(C_s)$ and $\Delta_{\perp} = 15300$ cm$^{-1}$ for $Ni^{+}(C_i)$.

For $Ni^{+}(C_i)$ electric dipole transitions between states of the $d^9$ configurations are completely forbidden. At the same time, for $Ni^{+}(C_s)$ the interdiction on parity is removed and, consequently, it was possible to expect occurrence of absorption bands in the region of 7000–14000 cm$^{-1}$ after an irradiation of crystals. Indeed, after irradiation of $BeAl_2O_4$: Ni samples, the bands connected with $Ni^{2+}(C_s)$ decrease and absorption at ~25000, 19000 and 9000 cm$^{-1}$ grows. However, it was impossible to distinguish bands of absorption with $\Delta_{||}$ and $\Delta_{\perp}$ overlapped by intense bands from $Ni^{2+}(C_s)$ and $Ni^{3+}(C_s)$. As the EPR spectra from $Ni^{2+}$ and $Ni^{3+}$ at frequency 9.3 GHz and 77 K were not observed, further study of the valence and coordination of Ni ions in beryl and chrysoberyl crystals is based on optical absorption spectra.

## Optical absorption spectra

### *$Be_3Al_2Si_6O_{18}$: Ni*

In beryl crystals doped with Ni ions, by analogy to Co ions (Solntsev et al. 2004), it was worthwhile to expect $Ni^{2+}$ and $Ni^{3+}$ in octahedral and $Ni^{2+}$ in tetrahedral sites. As it was already marked above, the difficulty in determining the coordination of Ni ions from the optical spectra arises from the fact that the absorption bands of Ni ions in octahedral and tetrahedral sites are localized in the same regions, 6000–8000 cm$^{-1}$ [$^4T_{2g}$ ($^{V1}Ni^{3+}$), $^3T_{2g}$($^{V1}Ni^{2+}$), $^3T_2$($^{IV}Ni^{2+}$)] and 12000–14000 cm$^{-1}$ [$^3T_{1g}$($^{V1}Ni^{2+}$) and $^3A_2$($^{IV}Ni^{2+}$)]. Taking this into account, we studied optical spectra of the crystals grown by different methods in which the ratios of contents of different ions are also different. Spectra of these crystals are represented in Fig. 3.

The analysis of optical absorption spectra of Ni ions in beryl crystals grown by flux-, hydrothermal- and gas-transport methods, as well as EPR data, points to the presence of three different Ni centres. Intense bands with maxima at 21740($\sigma$), 17240($\pi$), 9260($\sigma$) and 7140($\pi$) cm$^{-1}$, by analogy with $Co^{2+}$ (Solntsev et al. 2004) in beryl are identified with *dd* transitions $Ni^{3+}$ in octahedral $Al^{3+}$ site. The additional bands, most appreciable in hydrothermal beryl, with maxima at 25640($\sigma$ + $\pi$), 22220($\pi$); 13520($\pi$), 13160($\sigma$); and 8930($\sigma$), 7460($\pi$) cm$^{-1}$ are identified with $^3A_{2g} \rightarrow {}^3T_{1g}(P)$, $^3T_{1g}(F)$ and $^3T_{2g}(F)$ transitions of $Ni^{2+}$ in octahedral $Al^{3+}$ site ($^{V1}Ni^{2+}$), respectively. According to the EPR data, a part of $Ni^{+}$ and, hence, $Ni^{2+}$ ions occupy the $Be^{2+}$ sites. Considering this and the fact that after the $\gamma$-irradiation the intensity of optical bands in the region 15000–18000 and 6000–7000 cm$^{-1}$ decreased, the bands 17540($\sigma$), 15500($\pi$) and 6580($\sigma$ + $\pi$), 5950($\pi$) were attributed to $^3T_1(F) \rightarrow {}^3T_1(P)$ and $^3T_2(F)$ transitions of $Ni^{2+}$ ($^{IV}Ni^{2+}$) in tetrahedral $Be^{2+}$ site.

### *$BeAl_2O_4$: Ni*

According to the EPR data, $Ni^{+}$ and, consequently, $Ni^{2+}$, occupy octahedral sites with $C_i$ and $C_s$ symmetry in the chrysoberyl structure. In general, if the ion site possesses inversion symmetry, electric dipole transitions between states of the *d* configurations are forbidden. As a consequence, $Ni^{+}$($Ni^{2+}$, $Ni^{3+}$) that resides on an inversion site will have week magnetic-dipole no-phonon and phonon transitions. Therefore, here we shall discuss only $Ni^{2+}$ and $Ni^{3+}$ in a site with mirror symmetry.

The comparison of optical absorption spectra of Ni-doped flux (Fig. 4) and melt chrysoberyl crystals (Fig. 1, Gusev et al. 1988) allows allocating two types of the Ni centres. The first and more intense spectra of optical absorption in polarized light are typical of $Ni^{2+}$ in octahedral coordination (Pappalardo et al. 1961a, b). It has $^3T_1(P)$ bands peaking around 25500, 25900 and 26180 cm$^{-1}$; $^3T_1(F)$ bands with the maxima around 15680, 15720, 16000 cm$^{-1}$; and $^3T_2(F)$ bands with the maxima around 9570, 9430 and 9140 cm$^{-1}$ for the polarizations **E** || **c**, **E** || **a** and **E** || **b**, respectively. The second centre of Ni has week absorption bands that are shifted to longer wavelengths in comparison with the absorption bands of the first centre. Considering the fact that after an X-ray irradiation of samples the bands of $Ni^{2+}$ ions decreased and the bands close 25000 and 19000 cm$^{-1}$ grew in intensity (Fig. 4b), the latter have been identified as $^4T_{1g}(F) \rightarrow {}^4T_{1g}(P)$ and $^4A_{2g}(F)$ transitions of $Ni^{3+}$ ions at the octahedral $Al^{3+}(C_s)$ site, respectively. The third transition of $Ni^{3+}$ ($^4T_{1g} \rightarrow {}^4T_{2g}$) occurs in the absorption region of $Ni^{2+}$ ($^3A_{2g} \rightarrow {}^3T_{2g}$) and $Ni^{+}$ ($^2E \rightarrow {}^2T$).

The appearance of $Ni^+$ ions in irradiated $BeAl_2O_4$: Ni crystals can be explained as follows. A part of the electrons dislodged by X-ray quantum from oxygen ions immediately recombines to irradiate in ionized luminescence centres, whereas the other part is entrapped by various traps, including $Ni^{2+}$ ions. This leads to the formation of $Ni^+$ ions. This reaction is more probable than $Ni^{2+} + h\nu \rightarrow Ni^{3+} + \bar{e}$ and $Ni^{2+} + \bar{e} \rightarrow Ni^+$, because the concentration of oxygen centres is approximately three orders of magnitude higher than that of nickel centres. The compensation of the lacking charge in octahedral sites can be accomplished either by excess (superstoichiometric) $Be^{2+}$ ions in an empty tetrahedron or by $Al^{3+}$ ions in the $Be^{2+}$ sites. The latter alternative is confirmed by the fact that after the $\gamma$-irradiation of $BeAl_2O_4$: Ni crystals, in addition to $Ni^+$ centres at 77 K, we observed an EPR centre of "hole" type (Gusev et al. 1988; Solntsev et al. 2004). The centre is identified with hole ($O^-$) of one oxygen of $BeO_4$ tetrahedron in which Be is replaced by Al.

To process spectra, we made our calculations using the energy matrix of $d^3(d^7)$ and $d^2(d^8)$ electrons, considering $V_{cub} + V_{ee} + \alpha L(L+1) + V_{trig}$ (Sviridov et al. 1976; Veremeichik et al. 1977; Rahman and Runciman 1971) in the strong cubic field approximation. Term $\alpha$ takes into account interconfiguration or orbit–orbit interaction (Trees 1951, 1952). As the first step in analysis of optical spectrum of $Ni^{3+}$ and $Ni^{2+}$ ions in $Be_3Al_2Si_6O_{18}$ and $BeAl_2O_4$ crystals, the appropriate electrostatic and crystal field matrices were combined with trigonal crystal field matrices. The combined interaction matrices were diagonalized for different values of the Racah ($B$, $C$) octahedral crystal field parameter $\Delta(10\ Dq)$ and trigonal field parameters $v$, $v'$. The dependence of energy of various bands on these parameters was then examined. The calculation of low-symmetry spectra of $^{VI}Ni^{2+}$ and $^{VI}Ni^{3+}$ in chrysoberyl was performed in trigonal approach. The symmetry of $C_s$-monoclinic distorted octahedral $AlO_6$ complex in chrysoberyl is close to trigonal ($C_3$), if minor contributions of lower symmetry fields are neglected (Solntsev et al. 2004). As was mentioned above, the symmetry of $BeO_4$ tetrahedron in chrysoberyl can be also regarded as close to $C_3$. It is more difficult to present pseudotrigonal distortion of $BeO_4$ polyhedron in beryl structure at $Ni^{2+} \rightarrow Be^{2+}$ replacement. Therefore, calculation of $^{IV}Ni^{2+}$ levels in beryl is carried out in cubic (Table 5, calculation A) approximation. However, taking into account the fact that the EPR spectrum of $Ni^+$ had symmetry close to axial (unaxiality, i.e. $g_x - g_y$ was very small), it is possible

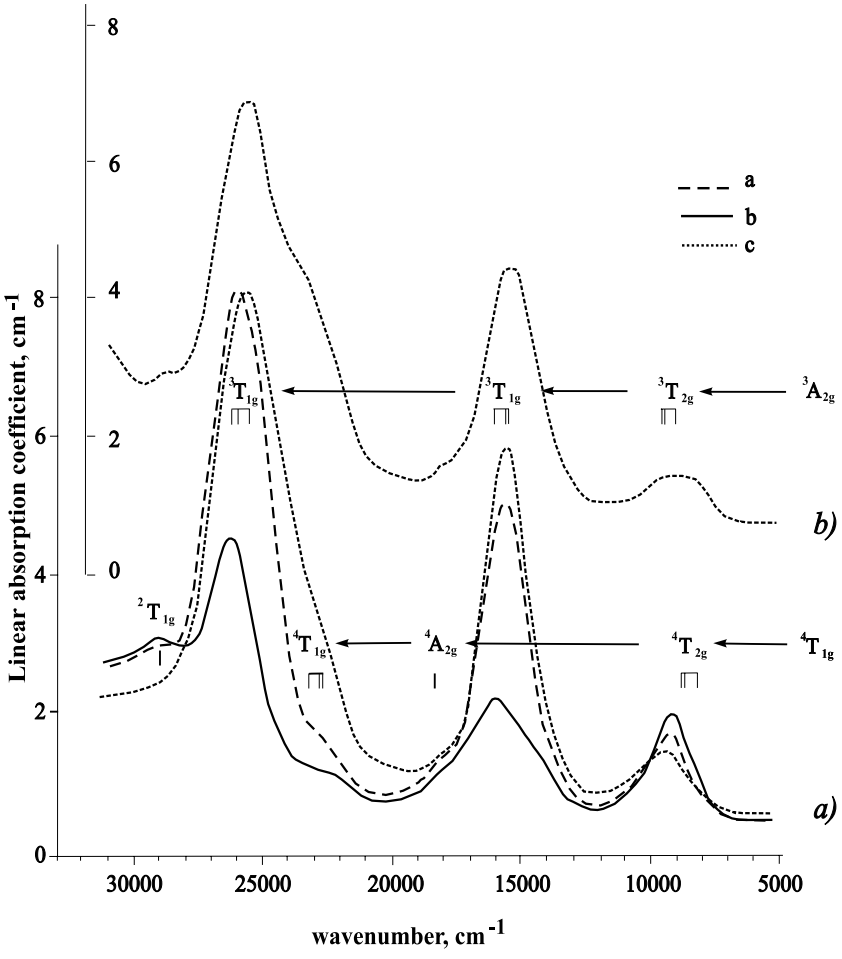


**Fig. 4** Polarized electronic absorption spectra of Ni-doped chrysoberyl at 300 K: *a* prior to irradiation, *b* after an X-ray irradiation (**E** || **c**)

to assume that the symmetry of a crystal field of $^{IV}Ni^{2+}$ is also close to axial. Thus, we can calculate the parameters of crystal field of $Ni^{2+}$ in pseudotrigonal approximation (Table 5, calculation B). The splitting of the energy levels of $Ni^{3+}$ in octahedral and $Ni^{2+}$ in octahedral and tetrahedral sites with different distortions are shown in (Solntsev et al. 2004, Fig. 4), and Figs. 5 and 6, accordingly. The selection rules for electric dipole transitions in the $Ni^{3+}$($Ni^{2+}$) ions in crystalline fields of $D_3$, $D_2$ and $C_s$ symmetry are given previously (Solntsev et al. 2004, Table 3). Observed and calculated electronic energy levels for the $Ni^{3+}$($Ni^{2+}$) ions in octahedral and tetrahedral sites are listed in Tables 3, 4 and 5 and graphically represented in Figs. 3 and 4.

## Discussion

In octahedral symmetry, $Ni^{3+}$ ions has a ground state $^4T_{1g}(F)$ and the lowest $d$–$d$ excited states are $^4T_{2g}(F)$, $^4A_{2g}(F)$ and $^4T_{1g}(P)$. Clearly, in $O_h$ symmetry there are only three spin-allowed transitions, i.e. those to quartet states $^4T_{2g}(F)$, $^4A_{2g}(F)$ and $^4T_{1g}(P)$. Under the perturbation $O_h \rightarrow D_{3d} \rightarrow D_3$ (beryl) or $O_h \rightarrow D_{3d} \rightarrow C_s$ (chrysoberyl) the degeneracy of these states is removed (Fig. 4, Solntsev et al. 2004). The $^4T_{1g}(F)$ term of ions with $d^7$ an electronic configuration ($Ni^{3+}$, $Co^{2+}$) in octahedral site is split into $^4E$ and $^4A$ levels in the trigonal field ($D_3$) of beryl. At a certain ratio of parameters $v$ and $v'$ the degeneracy of $^4T_{1g}(F)$ term is not removed. At minor splitting of $^4T_{1g}(F)$ term, the polarization of $Ni^{3+}$($Co^{2+}$) spectrum is determined by either $^4E$ or $^4A_2$ ground states (Solntsev et al. 2004). Thus, for the ground state the $^4E$ position of energy levels of $^{VI}Ni^{3+}$ in beryl is well described by parameters $Dq = 875$, $B = 840$, $C = 3880$, $v = 2970$, $v' = -1780$, $\alpha = 187$ cm$^{-1}$ (Table 3, calculation A). However, for the ground state $^4A_2$, the calculated values of energy levels $^{VI}Ni^{3+}$ (Table 3, calculation B) are in much poorer agreement with experimental data and do not explain polarizing dependence (Solntsev et al. 2004). Spin–orbit coupling leads to the following splitting: $^4A_2 \rightarrow E_{1/2} + E_{3/2}$, $^2E \rightarrow E_{1/2} + E_{3/2}$, $^2T_1 \rightarrow 2E_{1/2} + E_{3/2}$, $^2T_2 \rightarrow 2E_{1/2} + E_{3/2}$, $^2A_1 \rightarrow E_{1/2}$, $^2A_2 \rightarrow E_{1/2}$, $^4E \rightarrow 3E_{1/2} + E_{3/2}$. Calculation of this splitting in the approximation of cubic field in the first order yields splitting of $^4T_{1g}(F)$, $^4T_{2g}(F)$ and $^4T_{1g}(P)$ terms into three levels (Pappalardo et al. 1961a, b), each with shifts ($\zeta = -715$ cm$^{-1}$): $^4T_{1g}(F) = -842, -337, 505$ cm$^{-1}$, $^4T_{2g}(F) = -179, 119, 298$ cm$^{-1}$, $^4T_{1g}(P) = -327, 218, 544$ cm$^{-1}$. For the ground state $^4E_{1/2}$, transitions $E_{1/2} \rightarrow E_{1/2}$ are allowed in ($\pi + \sigma$), while $E_{1/2} \rightarrow E_{3/2}$, in $\sigma$-polarization; for the ground state $^4E_{3/2}$, transitions $E_{3/2} \rightarrow E_{1/2}$ in $\sigma$- and $E_{3/2} \rightarrow E_{3/2}$ are allowed in $\pi$-polarization. The calculated values for the energy of $Ni^{3+}$ levels agree well with experimental results (Table 3, calculation A).

When the symmetry of octahedral position is reduced to $C_s$ ($^{VI}Ni^{3+}$ in chrysoberyl), $E$-levels are split and $A''$ will be the ground state (Solntsev et al. 2004). The $A'' \rightarrow A'$ transitions are allowed in $Z$-polarization, while $A'' \rightarrow A''$, in $X$- and $Y$-polarization. The spin–orbit interaction causes additional splitting of levels. The $E'_{1/}$

**Table 3** Calculated and observed absorption bands of $Ni^{3+}$ in octahedral sites of beryl and chrysoberyl

| Beryl | | | | | | Chrysoberyl | | | | |
|---|---|---|---|---|---|---|---|---|---|---|
| Term ($O_h$) | Level ($D_3$) | Experiment | $\parallel$ **c**<br>$\perp$ **c** | Calculation | | Level ($C_s$) | | Experiment | $\parallel$ **c**<br>$\parallel$ **a**<br>$\parallel$ **b** | Calculation C |
| | | | | A | B | | | | | |
| $^4T_{1g}$ ($F$) | $E$ | | | 0 | 1907 | $A''$ | $A'$ | | | 1442 |
| | $A_2$ | | | 865 | 0 | $A''$ | | | | 0 |
| $^4T_{2g}(F)$ | $E$ | 7140 | $\parallel + \perp$ | 7606 | 9418 | $A''$ | $A'$ | 9090 | $\parallel$ **c** | 9653 |
| | $A_1$ | 9260 | $\perp + \parallel$ | 9272 | 8141 | | $A'$ | 9090 | $\parallel$ **a** | 9653 |
| | | | | | | | | 8480 | $\parallel$ **b** | 9434 |
| $^2E_g(G)$ | | | $\parallel + \perp$ | 8541 | 10340 | $A''$ | $A'$ | | | 9648 |
| $^4A_{2g}(F)$ | | 16000 | $\perp$ | 15923 | 19775 | $A''$ | | 18870 | $\parallel$ **a**<br>$\parallel$ **c** | 18802 |
| $^2T_{1g}(G)$ | $A_2$ | 16800 | $\parallel$ | 16285 | 16310 | $A''$ | $A'$ | | | 17543 |
| | $E$ | | | 17545 | 17353 | $A''$ | | | | 17707 |
| $^2T_{2g}(G)$ | $A_1$ | 16450 | $\parallel$ | 16024 | 18911 | | | | | 17726 |
| | $E$ | | | 16656 | 18585 | | | | | 22917 |
| $^4T_{1g}(P)$ | $E$ | 17240 | $\parallel + \perp$ | 17242 | 21552 | $A''$ | $A'$ | 23260 | $\parallel$ **b** | 23601 |
| | $A_2$ | 21740 | $\perp$ | 21759 | 17019 | $A''$ | | 22730 | $\parallel$ **a** | 22107 |
| | | | | | | | | 22730 | $\parallel$ **c** | 22107 |
| $^2T_{1g}(H)$ | $E$ | | | 21751 | 22462 | $A''$ | $A'$ | | | 18788 |
| | $A_2$ | | | 21867 | 22835 | $A''$ | | | | 22573 |
| $^2A_{1g}(G)$ | | 24100 | $\perp$ | 24087 | 23535 | $A'$ | | | | 25089 |
| $^2T_{1g}(F)$ | $E$ | 26040 | $\perp$ | 23217 | 25530 | $A''$ | $A'$ | 29070 | $\parallel$ **b** | 28947 |
| | $A_2$ | | | 27241 | 28038 | $A''$ | | | | 28902 |

Calculation A: $Dq = 875$, $B = 840$, $C = 3880$, $v = 2970$, $v' = -1780$, $\alpha = 187$ (cm$^{-1}$)
Calculation B: $Dq = 890$, $B = 850$, $C = 3960$, $v = -2990$, $v' = 960$, $\alpha = 38$ (cm$^{-1}$)
Calculation C: $Dq = 970$, $B = 940$, $C = 3960$, $v = -300$, $v' = -1040$, $\alpha = 0$ (cm$^{-1}$)

**Table 4** Calculated and observed absorption bands of $Ni^{2+}$ in octahedral sites of beryl and chrysoberyl

| Beryl | | | | | | Chrysoberyl | | | | |
|---|---|---|---|---|---|---|---|---|---|---|
| Term ($O_h$) | Level ($D_3$) | Experiment | \|\| **c**<br>⊥ **c** | Calculation | | Level ($C_s$) | | Experiment | \|\| **c**<br>\|\| **a**<br>\|\| **b** | Calculation C |
| | | | | A | B | | | | | |
| $^3A_{2g}$ ($F$) | | | | 0 | 0 | | | | | 0 |
| $^3T_{2g}(F)$ | $A_1$ | 7460 | \|\| | 8921 | 7551 | $A''$ | | 9140 | \|\| **b** | 9209 |
| | $E$ | 8930 | ⊥ + \|\| | 7479 | 8652 | $A'$ | | 9430 | \|\| **a** | 9352 |
| | | | | | | $A'$ | | 9570 | \|\| **c** | 9352 |
| $^3T_{1g}(F)$ | $E$ | 13160 | ⊥ + \|\| | 13259 | 14123 | $A''$ | | 15680 | \|\|**c** | 15158 |
| | $A_2$ | 13520 | \|\| + ⊥ | 13526 | 13454 | $A'$ | | 15720 | \|\| **a** | 15158 |
| | | | | | | $A''$ | | 16000 | \|\|**b** | 15458 |
| $^1E_g(D)$ | | | | 13598 | 13842 | $A''$ | $A'$ | | | 14152 |
| $^1T_{2g}(D)$ | $A_1$ | | | 22235 | 20926 | $A''$ | $A'$ | | | 22894 |
| | $E$ | | | 20681 | 22177 | $A''$ | | | | 23171 |
| $^3T_{1g}(P)$ | $A_2$ | 22220 | \|\| + ⊥ | 25687 | 22100 | $A''$ | $A'$ | 25500 | \|\| **c** | 25550 |
| | $E$ | 25640 | ⊥ + \|\| | 22209 | 25329 | $A''$ | | 25900 | \|\|**a** | 26283 |
| | | | | | | | | 26180 | \|\| **b** | 26283 |
| $^1T_{1g}(G)$ | $A_2$ | | | 26381 | 25371 | $A''$ | $A'$ | | | 27413 |
| | $E$ | | | 25170 | 26664 | $A''$ | | | | 27549 |
| $^1A_{1g}(G)$ | | | | 27479 | 28701 | | | | | 30538 |
| $^1T_{2g}(G)$ | $E$ | | | 33795 | 31046 | $A''$ | $A'$ | | | 34512 |
| | $A_1$ | | | 30694 | 34771 | $A''$ | | | | 35287 |

Calculation A: $Dq = 800$, $B = 830$, $C = 3750$, $v = -2560$, $v' = -760$, $\alpha = 0$ ($cm^{-1}$)
Calculation B: $Dq = 835$, $B = 860$, $C = 3750$, $v = 2520$, $v' = 590$, $\alpha = 0$ ($cm^{-1}$)
Calculation C: $Dq = 930$, $B = 892$, $C = 3750$, $v = 290$, $v' = 240$, $\alpha = 0$ ($cm^{-1}$)

$_2 \rightarrow E'_{1/2}$ transitions in this case will be allowed in $X$-, $Y$- and $Z$-polarization, which was observed in the experiments (Table 3, calculation C). The levels of $^{VI}Ni^{2+}$ energy in chrysoberyl with optimal parameters ($Dq = 970$, $B = 940$, $C = 3960$, $v = -300$, $v' = -1040$ and $= 0$ $cm^{-1}$), calculated in the approximation of trigonal field, qualitatively describe the experimental spectrum.

The three main bands observed at room temperature for each of the $Ni^{2+}$ spectra are transitions from the ground state $^3A_{2g}(F)$ to the excited states $^3T_{2g}(F)$, $^3T_{1g}(F)$ and $^3T_{1g}(P)$ in octahedral field $O_h$ symmetry. Under the

**Table 5** Calculated and observed absorption bands of $Ni^{2+}$ in tetrahedral sites of beryl

| Term ($T_d$) | Level ($D_2$) | Experiment **E** \|\|, ⊥ **c** | | Calculation | |
|---|---|---|---|---|---|
| | | | | A | B |
| $^3T_1(F)$ | $B_1$ | | | 0 | 0 |
| | $B_2$ | | | | 2608 |
| | $B_3$ | | | | |
| $^3T_2(F)$ | $B_1$ | 5950 | \|\| | 5813 | 5607 |
| | $B_2$ | 6580 | ⊥ + \|\| | | 6854 |
| | $B_3$ | | | | |
| $^3A_2(F)$ | $A$ | 12100 | \|\| + ⊥ | 11513 | 12004 |
| $^1E(D)$ | | 12380 | \|\| + ⊥ | 12287 | 11854 |
| $^1T_2(D)$ | $B_1$ | | | 11763 | 14174 |
| | $B_2$ | | | | 14548 |
| | $B_3$ | | | | |
| $^3T_1(P)$ | $B_1$ | 15500 | \|\| | 16416 | 15765 |
| | $B_2$ | 17540 | ⊥ | | 17308 |
| | $B_3$ | | | | |
| $^1T_2(G)$ | $B_1$ | | | 18983 | 19517 |
| | $B_2$ | | | | 20010 |
| | $B_3$ | | | | |
| $^1A_1(G)$ | | | | 20711 | 22759 |
| $^1T_1(G)$ | $B_1$ | | | 20883 | 21226 |
| | $B_2$ | | | | 23194 |
| | $B_3$ | | | | |
| $^1E(G)$ | | | | 24159 | 25306 |

Calculation A: $Dq = 570$, $B = 760$, $C = 3430$, $v = 0$, $v' = 0$, $\alpha = 0$ ($cm^{-1}$)

Calculation B: $Dq = 550$, $B = 730$, $C = 3430$, $v = 2700$, $v' = -70$, $\alpha = 0$ ($cm^{-1}$)

perturbation $O_h \rightarrow D_{3d} \rightarrow D_3$ (beryl) or $O_h \rightarrow D_{3d} \rightarrow C_s$ (chrysoberyl) the degeneracy of these states is removed, as represented in Fig. 5. Thus, in the group $D_3$ the electric dipole selection rules are $A_1, A_2 \leftrightarrow E(\sigma)$, $A_1 \leftrightarrow A_2\ (\pi)$, whereas $A_2 \leftrightarrow A_2$ is forbidden.

In the group $D_{3d}$, however, considering trigonally distorted $ML_6$ complexes, all the above transitions are vibronically allowed in either polarization (Lever and Hollebone 1972). In the case of beryl, the appearance of $^3A_{2g} \rightarrow {}^3A_{2g}$ ($^{V1}Ni^{2+}$) or $^4A_{2g} \rightarrow {}^4A_{2g}$ ($^{V1}Ni^{3+}$) transitions may infer a vibronic contribution or a strong $C_3$ component to the field. Assuming that these transitions were electronic, rather than vibronic, polarizing dependence of bands can be explained in terms of the spin–orbit interaction (Fig. 5). Spin–orbit coupling leads to the following splitting: $^1A_1 \rightarrow A_1$, $^1A_2 \rightarrow A_2$, $^1E \rightarrow E$, $^3A_1 \rightarrow A_2 + E$, $^3A_2 \rightarrow A_1 + E$, $^3E \rightarrow A_1 + A_2 + 2E$. Calculation of this splitting in the approximation of cubic field in the first order yields splitting of $^3T_{1g}(F)$, $^3T_{2g}(F)$ and $^3T_{1g}(P)$ terms into three levels each with shifts ($\zeta = -630\ cm^{-1}$): $^3T_{1g}(F) = 406, -406, -812\ cm^{-1}$, $^3T_{2g}(F) = 157, -157, -315\ cm^{-1}$, $^3T_{1g}(P) = -223, 223, 446\ cm^{-1}$. The spin–orbit interaction splits the ground level $^3A_2$ into a singlet ($A_1$) and a doublet ($E$), which are separated by a small magnitude of $D$ (a second-order effect of spin–orbital interaction). For the ground level $E$ transitions $E \rightarrow E$ are allowed in $(\pi+\sigma)$-, whereas $E \rightarrow A_1$, $A_2$, in $\sigma$-polarization (Fig. 5); for the ground level $A_1$ transitions $A_1 \rightarrow E$ are allowed in $\sigma$- and $A_1 \rightarrow A_2$ in $\pi$-polarization. At small $D$ values (of about a few $cm^{-1}$), transitions from both lower to upper levels are possible (Fig. 5). It complicated exact definition of the most preferable polarization for the given direction of a vector $\mathbf{E} \parallel \mathbf{c}$ or $\mathbf{E} \perp \mathbf{c}$. Therefore, calculation of parameters of a crystal field is carried out for two variants of an arrangement of levels of energy $Ni^{2+}$: (1) {$^3T_{2g}(F)$: $A_1 = 8930$, E = 7460; $^3T_{1g}(F)$: $A_2 = 13520$, $E = 13160$; $^3T_{1g}(P)$: $A_2 = 25640$, $E = 22220\ cm^{-1}$ (Table 4, calculation A)}; (2) {$^3T_{2g}$: $A_1 = 7460$, $E = 8930$; $^3T_{1g}$: $A_2 = 13160$, $E = 13520$; $^3T_{1g}$: $A_2 = 22220$, $E = 25640\ cm^{-1}$ (Table 4, calculation B)}. The calculated values for the energy of $Ni^{2+}$

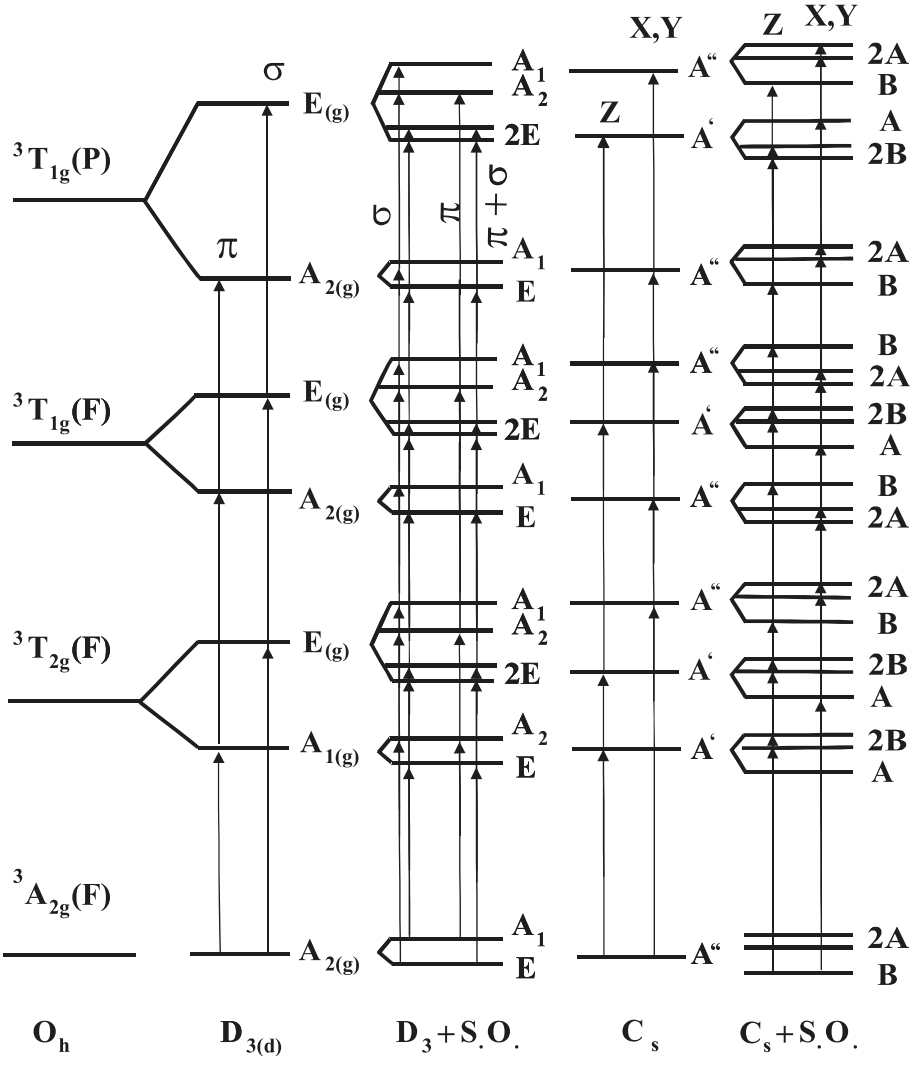


**Fig. 5** Scheme of splitting of energy levels of $Ni^{2+}$ in octahedral sites at deceasing symmetry of sites from $O_h \rightarrow D_{3d} \rightarrow D_3$ or $O_h \rightarrow D_{3d} \rightarrow C_s$ (for $D_3$ symmetry index "$g$" should be omitted)

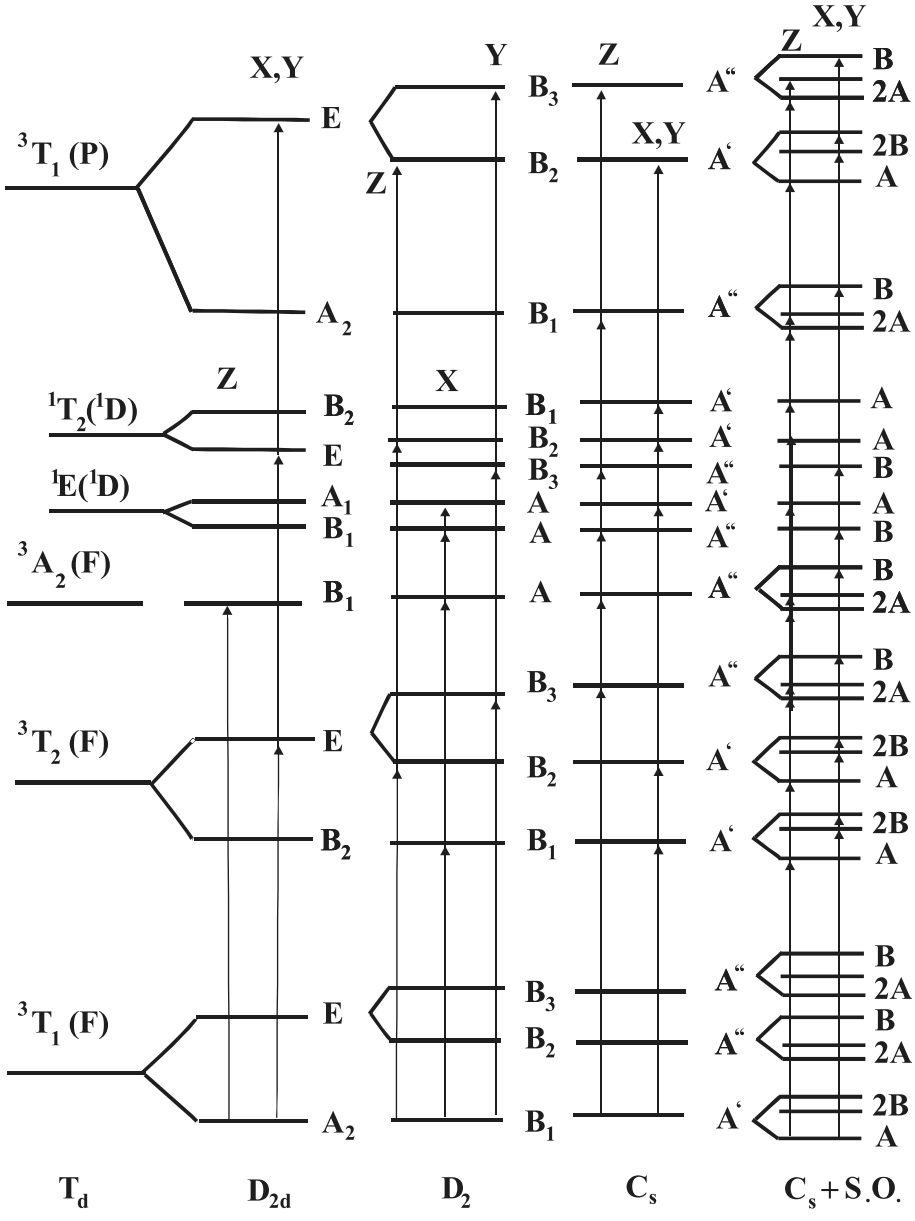


**Fig. 6** Scheme of splitting of energy levels of $Ni^{2+}$ in tetrahedral sites at decreasing symmetry of sites from $T_d \rightarrow D_{2d} \rightarrow D_2$ or $T_d \rightarrow D_{2d} \rightarrow C_s$

level agree well with experimental results (Table 4, calculation A).

When the symmetry of $AlO_6$ octahedron is reduced to $C_s$ ($Ni^{2+}$ in chrysoberyl), $E$-levels are split and $^3A''$ will be the ground state (Fig. 5). The transitions $^3A'' \rightarrow {}^3A'$ are allowed in $Z$-polarization, and $^3A'' \rightarrow {}^3A''$, in $X$- and $Y$-polarization (Solntsev et al. 2004). The spin–orbit interaction causes additional splitting of levels (Fig. 5). The $A \leftrightarrow B$ transitions in this case will be allowed in $X$-, $Y$-polarization and $A \leftrightarrow A$, $B \leftrightarrow B$, in $Z$-polarization. The symmetry of $AlO_6$ octahedron in chrysoberyl is close to trigonal ($C_3$), if minor contributions of fields of lower symmetry are neglected (Solntsev et al. 2004). The levels of $^{VI}Ni^{2+}$ energy in chrysoberyl with optimal parameters ($Dq = -930$, $B = 892$, $C = 3750$, $v = 290$, $v' = 240$ and $\alpha = 0$ cm$^{-1}$), calculated in the approximation of trigonal field, describe well the experimental spectrum.

As seen from Fig. 6 the lowest $^3T_1(F)$ term of $Ni^{2+}$ in tetrahedral site is split into $^3A_2$ (lower) and $^3E$ (upper) in crystal field $D_{2d}$ symmetry. In beryl, $Ni^{2+}$ replaces $Be^{2+}$ (point symmetry of site $D_2$). The ground state $B_1$ occurs in $D_2$ distorted tetrahedral $Ni^{2+}$ complexes. Transitions $B_1 \rightarrow A$, $B_3$ and $B_2$ are allowed in $X$-, $Y$- and $Z$-polarization, respectively (Table 2 in Solntsev et al. 2004). Thus, axis $X$ of the spectrum coincides with axis **c** || [0001] crystal and axis $Z$, with $[2\bar{1}\bar{1}0]$ || **a**. In this scheme it is difficult to explain the appearance of the band 15500 cm$^{-1}$ at **E** || **c** ($\pi$-polarization), as transitions $B_1 \rightarrow B_1$ are forbidden. This prohibition will be removed by spin–orbit interaction. Then transitions $A \rightarrow A$ and $B \rightarrow B$ are allowed in $\pi$-, and $A \rightarrow B$,

in $\sigma$ polarization. Calculation of splitting of the levels caused by spin–orbit coupling, in approximation of cubic crystal field in first order, shows that the $^3T_1(F)$, $^3T_2(F)$ and $^3T_1(P)$ terms split into three levels each: $^3T_1(F) = -900, -450, 450\ cm^{-1}$; $^3T_2(F) = -157, 157, 315\ cm^{-1}$; and $^3T_1(P) = -298, 298, 596\ cm^{-1}$.

Calculation of energy levels $^{IV}Ni^{2+}$ in beryl is carried out in cubic (Table 5, calculation A) approximation. For an estimation of anisotropy parameters of spectra $^{IV}Ni^{2+}$ calculation in trigonal approximation has been carried out (Table 5, calculation B). The ground level $^3A_2$ in trigonal crystal field is split into a singlet $A_1$ (lower) and a doublet $E$ (upper) by a second-order effect of the spin–orbit interaction. The evaluation of this splitting by formula (Rahman and Runciman 1971) $D \approx 5\zeta^2/7(3v + 2v') = 5\zeta^2/21\delta$ gives $D = 35.6\ cm^{-1}$ and explains why the EPR of $Ni^{2+}$ was not seen at frequency of 9.3 GHz. Here $\delta \approx v + 2/3\ v'$ is the splitting of the $^3T_1(F)$ ground term in a trigonal field, and $D$ is the splitting of the $^3A_2$ ground level by spin–orbit interaction.

In chrysoberyl, $Ni^{2+}$ ions, in addition to octahedral site of $Al^{3+}$, can also occupy tetrahedral sites of $Be^{2+}$ (point symmetry of the position is $C_s$). Transitions $A' \rightarrow A''$ are allowed in $Z$-polarization, and $A' \rightarrow A'$, in $X$- and $Y$-polarizations. In this case spin–orbit interaction also removes the prohibition of the transitions $A \rightarrow A$ ($Z$-polarization) $A \rightarrow B$ ($X$-, $Y$-polarization) (Fig. 6). However, as was mentioned above, no bands of absorption from $^{IV}Ni^{2+}$ in chrysoberyl were observed, probably, because of the low concentration of Ni ions in crystals (Table 1).

## Conclusions

Thus, the agreement of experimental and calculated locations of the $Ni^{3+}$ and $Ni^{2+}$ energy levels shows that the assignment of main absorption bands is reasonable. Polarization dependence of these bands can be explained only when spin–orbit interaction is taken into account.

Our spectroscopic studies evidence that Ni ions enter beryl structure in bi- and trivalent states, replacing octahedral sites of $Al^{3+}$ ($Ni^{3+}$, $Ni^{2+}$) and tetrahedral sites of $Be^{2+}$ ($Ni^{2+}$). In chrysoberyl, $Ni^{3+}$ and $Ni^{2+}$ replace octahedral sites of $Al^{3+}$. Thus, ~68% of these ions occupy $Al^{3+}$ sites with mirror symmetry and ~32%, sites with inversion symmetry.

The data obtained indicate that the lacking charge of $Ni^{2+}$ in octahedral sites of beryl is compensated by the appearance of $Al^{3+}$ in $Be^{2+}$ site. This is confirmed by the EPR observation of $O^-$ centres as well as $Al^{2+}$ centres in $Be^{2+}$ site after $\gamma$-irradiation of these crystals. The compensation of the lacking $Ni^{2+}$ charge in octahedral sites can be realized by either excess (superstoichiometric) $Be^{2+}$ ions in empty tetrahedron or by $Al^{3+}$ ions in the $Be^{2+}$ sites.

**Acknowledgements** We thank Dr. G.G. Khranenko, Dr. A.S. Lebedev (deceased), N.A. Novgorodtseva (deceased), and Dr. A.Ya. Rodionov for the kindly donation of samples used in this study. This work was supported by the Russian Foundation for Basic Research (Grant 06-05-64395).

## References

Aines RD, Rossman GR (1984) The high-temperature behavior of water and carbon dioxide in cordierite and beryl. Am Mineral 69:319–327

Alimpiev AI, Bukin GV, Matrosov VN, Pestryakov EV, Solntsev VP, Trunov VI, Tsvetkov EG, Chebotaev VP (1986) A tunable $BeAl_2O_4$: $Ti^{3+}$ laser (in Russian). Kvantovaya Electronika 14:885–886

Aurisicchio C, Fioravanti G, Grubessi O, Zanazzi PF (1988) Reappraisal of the chemistry of beryl. Am Mineral 73:826–837

Bakakin VV, Rylov GM, Belov NV (1967) Correlation between chemical composition and unit cell parameters of beryl (in Russian). Dokl Acad Sci USSR Earth Sci 173:129–132

Barry WR, Troup GI (1970) EPR of $Fe^{3+}$ ions in chrysoberyl. Phys Status Sol B 38:229–234

Bukin GV, Matrosov VN, Orekhova VR, Remigailo YuL, Sevastyanov BK, Symonov EG, Solntsev VP, Tsvetkov EG (1981) Growth of alexandrite crystals and investigation of their properties. J Crystal Growth 52:537–541

Carrington A, McLachlan AD (1970) Magnetic resonance and his application in chemistry. Mir, Moscow, 447 p (translated from Carrington A, McLachlan AD (1967) Introduction to magnetic resonance with applications to chemistry and chemical physics. Harper and Row Publishers, inc, New York)

Dvir M, Low W (1960) Paramagnetic resonance and optical spectrum of iron in beryl. Phys Rev 119:1587–1591

Edgar A, Vance ER (1977) Electron paramagnetic resonance, optical absorption and magnetic circular dichroism studies of $CO_3^-$ molecular-ion in irradiated natural beryl. Phys Chem Minerals 1:165–178

Farrell EF, Fang JH, Newnham RE (1963) Refinement of the chrysoberyl structure. Am Mineral 48:804–810

Feklichev VG (1963) Chemical composition of minerals of the beryl group (in Russian). Geokhimiya 3:391–401

Forbes CE (1983) Analysis of the spin-Hamiltonian parameters for $Cr^{3+}$ in mirror and inversion symmetry sites of alexandrite ($Al_{2-x}Cr_xBeO_4$). Determination of the relative site occupancy by EPR. J Chem Phys 79:2590–2599

Hayes W, Wilkens J (1964) Proc Roy Soc. London Ser A 281:340–345

Hoffmann SK, Goslar J (1982) Crystal field theory and EPR parameters in $D_2$ and $C_{2v}$ distorted tetrahedral copper (II) complexes. J Solid State Chem 44:343–353

Geusic IE, Peter M, Schulz-du-Bois OE (1959) Paramagnetic resonance spectrum of $Cr^{3+}$ in emerald. Bell Syst Techn J 38:291–296

Ginsburg DS (1955) On the question of the composition of beryl (in Russian). Trans Min Acad Sci USSR 7:56–69

Goldman DS, Rossman GR, Parkin KM (1978) Channel constituents in beryl. Phys Chem Minerals 3:225–235

Gulev VS, Eliseev AP, Solntsev VP, Khranenko GG, Yurkin AM (1987) Flash-lamp pumped laser using emerald grown by the flux method (in Russian). Kvantovaya Electronika 14:1990–1992

Gusev VA, Eliseev AP, Samoilova EG, Solntsev VP, Yurkin AM (1988) Optical and EPR spectroscopy of chrysoberyl crystals doped with nickel (in Russian). J Appl Spectrosc 48:772–778

Khranenko GG, Solntsev VP (1988) Isomorphous substitutions in synthetic beryls (in Russian). In: Trudy Instituta Geologii i Geofiziki, Akademiya Nauk SSSR, is 487. Novosibirsk, pp 94–99

Lebedev AS, Klyakhin VA, Solntsev VP (1988) Crystal chemistry features of hydrothermal beryls (in Russian). In: Trudy Instituta Geologii i Geofiziki, Akademiya Nauk SSSR, 708. Novosibirsk, pp 75–94

Lever ABP, Hollebone BP (1972) A theoretical study of the electronic spectra of trigonally distorted transition metal complexes. I. $d^1$, $d^3$, $d^8$, and $d^9$ complexes. J Am Chem Soc 94:1816–1823

Mashkovtsev RI, Solntsev VP (2002) Channel constituents in synthetic beryl: ammonium. Phys Chem Minerals 29:65–71

Morosin B (1972) Structure and thermal expansion of beryl. Acta Cryst B 28:1899–1903

Morton JR, Preston KF (1978) Atomic parameters for paramagnetic resonance date. J Magn Res 30:577–582

Pappalardo R, Wood DL, Linares RC (1961a) Optical absorption study of Co-doped oxide system. J Chem Phys 35:2041–2059

Pappalardo R, Wood DL, Linares RC (1961b) Optical absorption study of Ni-doped oxide system. J Chem Phys 35:1460–1478

Rahman HU, Runciman WA (1971) Energy levels and *g*-values of vanadium in corundum. J Phys C Solid State Phys 4:1576–1590

Rodionov AYa, Solntsev VP, Weis NS (1987) Crystallization and properties of colouring varieties of gas-transport beryl (in Russian). In: Trudy Instituta Geologii i Geofiziki, Akademiya Nauk SSSR, 679 Novosibirsk, pp 41–53

Rodionov AYa, Novgorodtseva NA (1988) Crystallization of the colored varieties of chrysoberyl by the solution-melt and gas-transport methods (in Russian). In: Trudy Instituta Geologii i Geofiziki, Akademiya Nauk SSSR, 708 Novosibirsk, pp 182–187

Shand ML, Chine CF (1982) A tunable emerald laser. IEEE J Quantum Electron QE-18:1829–1830

Solntsev VP (1981) The nature of colour centers and EPR in beryl and chrysoberyl (in Russian). In: Trudy Instituta Geologii i Geofiziki, Akademiya Nauk SSSR, 499. Novosibirsk, pp 92–140

Solntsev VP, Khranenko GG (1989) The EPR of radiation defects in beryl. Sov Phys Solid State 31:292–295

Solntsev VP, Lebedev AS, Pavlyuchenko VS, Klyakhin VA (1976) Copper centers in synthetic beryl (in Russian). Sov Phys Solid State 46:1396–1398

Solntsev VP, Tsvetkov EG, Alimpiev AI, Mashkovtsev RI (2004) Valent state and coordination of cobalt ions in beryl and chrysoberyl crystals. Phys Chem Minerals 31:1–11

Sviridov DT, Sviridova RK, Smirnov YuF (1976) Optical spectra of transition metal ions in crystals (in Russian). USSR, Nauka, Moscow, 266 p

Trees RE (1951) Configuration interaction in Mn (II)**.** Phys Rev 83:756–760

Trees RE (1952) The $L(L+1)$ correction to the Slater formulas for the energy levels. Phys Rev 85:382

Tsvetkov EG (1982) Growth and investigation of some properties of the crysoberyl crystals (in Russian). PhD Thesis, Institute of Geology and Geophysics SB RAS USSR

Veremeichik TF, Grechushnikov BN, Kalinkina IN, Sviridov DT (1977) Trees correction for $d^3$-configuration in a strong field scheme. Configuration of $d^3$-electron in trigonal field (in Russian). Z Prikladnoi Spektrosk 26:131–136

Walling JC, Peterson OG, Jenssen HP, Morris RC, O′Dell EW (1980) Tunable alexandrite lasers. IEEE J Quantum Electron QE-16:1302–1314

Wood DL, Nassau K (1968) The characterization of beryl and emerald by visible and infrared absorption spectroscopy. Am Mineral 53:777–800